Comparison of Narrow Bipolar Events with ordinary lightning as proxies for severe convection

Abram R. Jacobson (corresponding author)
ISR-2
Mail Stop D436
Los Alamos National Laboratory
Los Alamos, New Mexico 87545 (USA)
ajacobson@lanl.gov 505-667-9656 fax 505-664-0362

and

Mathew J. Heavner
Department of Physics
University of Alaska Southeast
11120 Glacier Highway, Juneau, AK 99801

This manuscript will be submitted to the journal Monthly Weather Review published by the American Meteorological Society.

Abstract

Narrow Bipolar Events (NBEs) are a recently studied intracloud electrical-discharge process. It is speculated that an NBE is instigated by the extensive atmospheric shower of an energetic cosmic ray. NBEs cause significant relaxation of the charge separation within the electrified cloud in a short time, on the order of 10 μs. The current flow causes radiation of a distinctive "bipolar" low-frequency/very-low-frequency signal that can be recorded at locations on Earth up to thousands of km from the source. NBEs are preceded/accompanied by the most powerful very-high-frequency radio emissions seen in any kind of lightning. These intense pulsed radio emissions have been routinely detected with satellite-borne radio receivers in space. Owing to their easy detection and recognition, NBEs might be a useful remote-sensing proxy for space-based global, near-real-time remote sensing. However, in order for that potential to be realized, NBEs must be shown to be associated, as is ordinary lightning, with severe tropospheric convection, rather than to be just a curiosity of cosmic-ray/atmosphere interactions. We address this question with a detailed comparison of NBEs and ordinary lightning using a ground-based lightning-transient research facility that records signals from both ordinary lightning and NBEs, the Los Alamos Sferic-waveform Array (LASA), based in Florida. First, the data from LASA are internally compared to examine the relationship of NBEs and ordinary lightning in both position and time. Second, we examine the relationship of both NBEs and ordinary lightning to simultaneous infrared cloud imagery (from the GOES-East satellite) in order to infer the relative affinities of NBEs and ordinary lightning for cloud signatures that are consistent with severe convection.

1. Introduction and background

Space-based detection and location of lightning offers the potential for global, near-real-time monitoring and tracking of severe deep convection. Space-based remote sensing offers, in principle, unhindered access to the entire planet. Lightning can be monitored from space by satellite-based detection of both optical [Boccippio, D. J. et al., 2000: Christian, H. J. et al., 1999: Christian, H. J. et al., 1999: Kirkland, M. W. et al., 2001: Suszcynsky, D. M. et al., 2001: Suszcynsky, D. M. et al., 2000] and radio-frequency (RF) emissions [Jacobson, A. R. et al., 1999: Jacobson, A. R. et al., 2000: Light, T. E. L. and Jacobson, A. R., 2003: Shao, X.-M. and Jacobson, A. R., 2001: Shao, X.-M. and Jacobson, A. R., 2002].

Space-based RF monitoring of lightning can be done only at frequencies sufficiently high not to be blocked or overly dispersed by the ionosphere [Jacobson, A. R. et al., 1999: Massey, R. S. et al., 1998: Roussel-Dupré, R. A. et al., 2001]. In practice this means that the frequencies of observation must be in the Very High Frequency band (VHF; 30-300 MHz). The background of anthropogenic noise in the VHF forces lightning detection in space to exploit the most intense RF emissions, as only these can be triggered-upon while at the same time rejecting the high backgrounds of anthropogenic radio noise as seen from space. In addition, since space-based RF lightning *location* (as opposed to mere detection) relies on multi-satellite Time Difference Of Arrival (TDOA) methods [Suszcynsky, D. et al., 2000], it is preferable to work with narrow (a few μs) pulses.

There are essentially two classes of lightning RF pulses that are sufficiently narrow and intense to meet these two requirements. The first of these pulse types is radiated by the initiation of negative cloud-to-ground (-CG) return strokes on seawater [Jacobson, A. R. and Shao, X.-M., 2002]. The second of these pulse types is the RF emission associated with an intracloud discharge process called a "Compact Intracloud Discharge" or CID [Smith, D. A. et al., 1999]. The CID is seen in the VHF but may sometimes precipitate a lower-frequency radiation called a "Narrow Bipolar Event", or NBE [Jacobson, A. R., 2003: Jacobson, A. R., 2003: Jacobson, A. R. and Light, T. E. L., 2003: Le Vine, D. M., 1980: Light, T. E. L. and Jacobson, A. R., 2003: Smith, D. A. et al., 1999: Willett, J. C. et al., 1989]. The CID emissions are the most intense thunderstorm emissions in the VHF and have been routinely detected from the ground [Thomas, R. J. et al., 2001], from low-Earth orbit [Jacobson, A. R. and Light, T. E. L., 2003: Light, T. E. L. and Jacobson, A. R., 2003: Massey, R. S. and Holden, D. N., 1995: Massey, R. S. et al., 1998], and from the Global Positioning System satellite constellation [Suszcynsky, D. et al., 2000] at 12-hour orbit. Henceforth we shall use the single term "NBE" to refer to both the more numerous CIDs (seen in VHF) and the less numerous NBEs that are seen in lower frequencies and that are precipitated by a CID. The intense RF pulse sometimes followed by a NBE is accompanied by less optical power than are the various non-NBE lightning processes [Jacobson, A. R., 2003: Jacobson, A. R., 2003: Jacobson, A. R. and Light, T. E. L., 2003: Light, T. E. L. and Jacobson, A. R., 2003]. The relationship of optical output to the NBE low-frequency discharge will be explored in a separate publication; for the present, suffice it to say that the low-frequency NBEs, like their VHF instigators, tend to be dark compared to ordinary lightning. Since light output is implied by the name

"lightning", evidently the NBE is an extraordinary form of lightning. Thus we shall distinguish NBEs and non-NBEs by calling all non-NBE's "ordinary lightning". Observations [Jacobson, A. R., 2003] are consistent with a possible role of energetic cosmic rays in the instigation of NBEs and their associated RF emissions, as proposed earlier [Gurevich, A. V. et al., 1999].

Figure 1 shows (a) positive polarity NBE, (b) negative-polarity NBE, and (c) ordinary-lightning vertical-electric-field signals as recorded by the Los Alamos Sferic-waveform Array (see Section 2 below). The initial pulse is bipolar and has a duration on the order of 10 □s, much shorter than the pulses seen with typical ordinary lightning. The delayed echoes on the NBE traces (Figures 1a and b) are due to ionospheric reflections and are the basis for LASA's emission-height estimates [Smith, D. A. et al., 2004].

Due to its higher intensity in the VHF band, RF signals associated with NBEs will be essential to space-based RF monitoring of thunderstorms. Therefore, it is necessary to assess the NBE's utility as a remote-sensing proxy for deep convection. Others have demonstrated that ordinary lightning can be a useful proxy for deep convection, albeit with systematic differences between diverse cloud regimes, e.g. oceanic versus continental, pristine versus aerosol-dominated, or monsoon versus break conditions [Boccippio, D. J., 2002: Boccippio, D. J. et al., 1999: Nesbitt, S. W. et al., 2000: Petersen, W. A. and Rutledge, S. A., 1998: Toracinta, E. R. and Zipser, E., 2001: Toracinta, E. R. et al., 2002: Ushio, T. et al., 2001: Williams, E. et al., 2002: Zipser, E. J., 1994: Zipser, E. J. and Lutz, K. R., 1994]. Thus, the key question to be addressed here is:

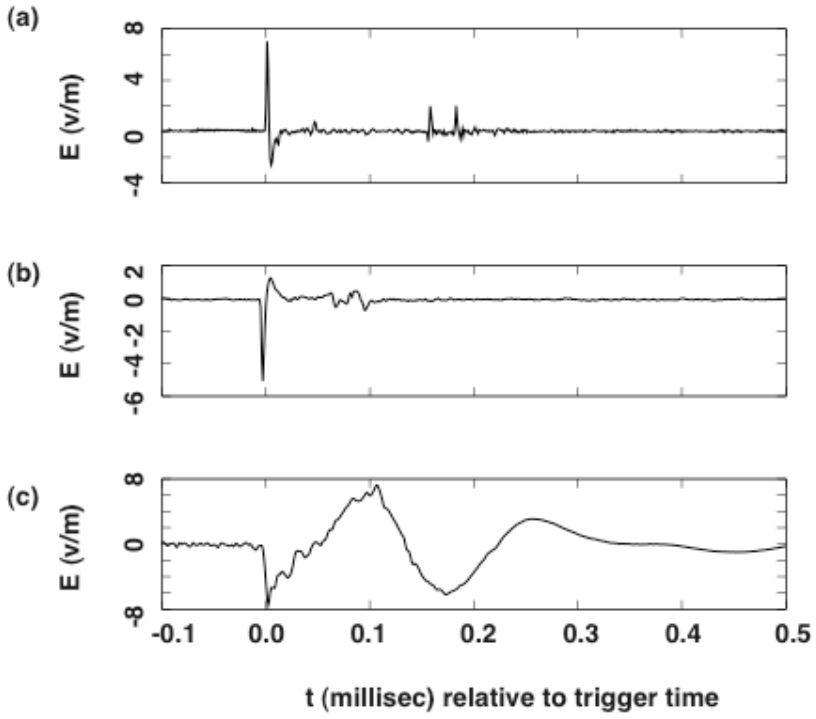

Figure 1: Vertical-electric-field waveforms recorded by the LASA ground-based facility (see text). (a) Positive NBE followed by ionospheric reflections. (b) Negative NBE followed by ionospheric reflections. (c) Non-NBE ("ordinary") lightning signal.

Do NBEs behave like ordinary lightning, and in particular, do NBEs share ordinary lightning's marked selectivity for severe tropospheric convection? If so, then NBEs might be a useful remote-sensing proxy for severe convection. Or are NBEs merely an aesthetically pleasing curiosity of nature (on a par with, e.g., a "sun dog") having little selectivity for severe convection? If the latter, then NBEs would not be a promising remote-sensing observable for global monitoring of severe convection.

2. Description of the data sources

The data used in this study comprise (a) recordings of lightning-discharge vertical-electric-field-change signals at ground level, and (b) inference of cloud-top temperature from satellite infrared cloud imagery. The data are focused on the Florida region. Specifically, the cloud imagery is stored for an 8-deg X 8-deg (longitude, latitude) box, and the lightning data is stored for a 400-km radius circle located within that box, both the box and the circle centered on –81.5 deg E longitude, 28 deg N latitude. Figure 2 shows the Florida area with the 400-km-radius circle superposed.

The data on lightning discharges are from the Los Alamos Sferic-waveform Array (LASA) [Smith, D. A. et al., 2002] in the Florida area during the four-year period 1999-2002. The array at various times during 1999-2002 (cumulatively, but not always simultaneously) comprised stations at the locations shown in Table 1. The data on any particular lightning discharge used here is accepted only if there are at least four stations

Table 1: LASA stations in Florida (cumulative over 1999-2002).

station name (abbreviation)	longitude (deg E)	latitude (deg N)
Boca Raton (br)	-80.1015	26.3733
Cape Kennedy (kc)	-80.6424	28.5386
Tampa (ta)	-82.4145	28.0598
Fort Myers (fm)	-82.0151	26.6346
Gainesville (gv)	-82.3472	29.6424
near Fort Myers (fy)	-81.8687	26.6441
Orlando (or)	-81.1960	28.5860
Daytona (da)	-81.0472	29.1891
Tallahassee (te)	-84.2994	30.4461
Key West (kw)	-81.6899	24.5816

Table 2: LASA locations of various lightning types for 1999-2002.
Required: 4 or more Florida stations participating in location.

+CG	-CG	undetermined	+NBE	-NBE
23,991	1,697,338	1,249,338	79,068	24,172

Table 3: LASA locations of lightning types for 1999-2002 with simultaneous GOES-East channel 4 infrared imagery.
Required: 4 or more Florida stations participating in location.

non-NBE (= +CG & -CG & undetermined)	NBE (= +NBE & -NBE)	NBE (= +NBE & -NBE) with height retrieval
1,001,347	32,556	20,933

Table 4: Equal-time, zero-separation, pixel-population correlation coefficients.
Data used are the full 1999-2002 dataset with 4 or more Florida stations participating in location (see Table 2).

undet., +NBE	undet., -NBE	undet., -CG	+NBE, -NBE	-CG, +NBE	-CG, -NBE
25%	26%	47%	11%	29%	16%

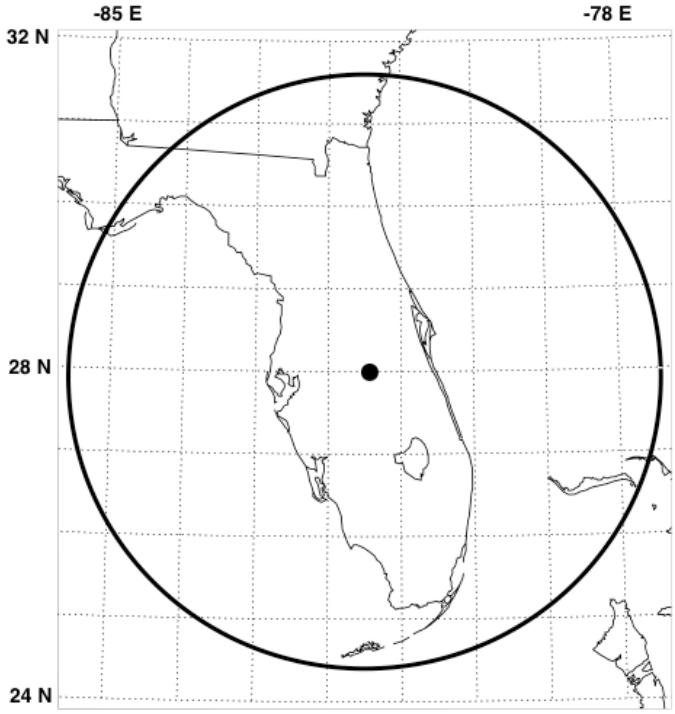

Figure 2: Map of Florida study area, with 400-km-radius circle centered on –81.5 E, 28.0 N. The lightning-location grid extends over 8 deg X 8 deg centered on this point, with 0.2-deg X 0.2-deg pixels.

participating in that particular lightning location. This allows at least four data points (waveform arrival times at stations) for the retrieval of three unknowns (longitude, latitude, and time of the lightning discharge). The degrees of freedom (≥ 1) allows assessment of the lightning-location errors and rejection of spurious solutions.

LASA is a research tool developed by the Los Alamos National Laboratory (LANL) for ground support of the FORTE satellite [Jacobson, A. R. et al., 1999] and of the radio sensors on the GPS satellites [Suszcynsky, D. et al., 2000]. The electric-field waveform is sampled at a rate of 1 megasample/s (so that the Nyquist bandpass is 0.5 MHz). Typically 8192 samples (8.192 millisec) of data are contained in a record for a single trigger. The LASA system returns full waveform records to the network headquarters (in Los Alamos, New Mexico) daily for analysis and attempted identification of the causative lightning process. The choices of lightning process include +NBE, -NBE, +CG, -CG, and "undetermined". The robotic identification of LASA-recorded waveforms is conservative, and most of the "undetermined" that are checked by eye appear to be probable ground strokes. For either polarity of NBE, the discharge height can often be determined [Smith, D. A. et al., 2004]. Both of these features –return of the full waveform, and retrieval of the emission height for some NBE discharges –are unique to LASA and not currently available in operational lightning-location systems based on signals in the low-frequency (30-300 kHz) and very-low-frequency (3-30 kHz) range. This ability to archive and to examine full waveforms is the reason for the LASA research facility. Table 2 indicates the number of each identified type of lightning discharges located by LASA within the 400-km-radius circle (see Figure 2) during the

four years of this study. Summing over the various types of identifications, there were 3,073,907 acceptable lightning locations during the 1999-2002 period.

The data on cloud-top temperature are derived from the GOES-East satellite's infrared (10.7 micron IR; channel #4) data made available by the National Oceanographic and Atmospheric Administration (NOAA). We download the entire hemispheric image (updated typically every 15 minutes) and archive the image at our LASA headquarters. The data are downloaded from the NASA Goddard Spaceflight Center FTP website (ftp://rsd.gsfc.nasa.gov/) automatically at the end of each day. During the period 1999-2002, we usually, but not always, succeeded in automatically archiving the cloud imagery. The satellite data was not always available even if the download was attempted. For this and other reasons, there are substantial gaps in the IR imagery archive used in this study. Furthermore, a threshold was set to exclude entire days having <10 LASA events within the 400-km-radius circle, even if the GOES-East data was in our archive. The IR data was considered useable for a given lightning discharge only if the IR was recorded within ± 15 minutes (900 s) of the lightning event's occurrence. Subject to these restrictions, the total number of accepted, IR-supported LASA events within the 400-km-radius circle was 1,054,836 during the period 1999-2002. This is about a third of the total number of lightning locations characterized by LASA within the 400-km-radius circle during that period. Table 3 indicates the breakout of these 1,054,836 IR-supported events in the overall categories of NBEs and non-NBEs, as well as the number of NBEs that provided automated emission-height retrieval [Smith, D. A. et al., 2002].

3. Relation of Narrow Bipolar Events to cloud-to-ground lightning discharges

A previous study [Suszcynsky, D. M. and Heavner, M. J., 2003] demonstrated two trends: First, the NBE occurrence rate statistically trends upward for Florida thunderstorms with higher flash rates of –CG or +CG lightning events. Second, the storms with higher flash rates of –CG or +CG lightning events also tend to have higher altitudes of NBE discharges. Each trend was shown to be statistically significant though with wide scatter. In the present study we will further examine the spatial and temporal relationship between the CG and NBE lightning events.

In order to compare the behavior of NBEs and CGs, we have divided the 8-deg X 8-deg study zone (see Figure 2) into 40 X 40 pixels (1600 pixels total), each pixel measuring 0.2-deg X 0.2 deg, or ~ 20-km (E-W) X 22-km (N-S). This is within a factor-of-two of the typical convective-cell size (~10 km) in either air-mass thunderstorms or multi-cellular fronts. We have divided time into windows of duration 10 minutes (600 s), advanced by half a window width (5 minutes, or 300 s). Thus each three-dimensional spatio-temporal data pixel is spaced by 20-km (E-W) X 22-km (N-S) X 300s. This compares with a spacing of 50-km X 50-km X 900s used previously [Suszcynsky, D. M. and Heavner, M. J., 2003]. The present study thus increases the three-dimensional spatio-temporal pixel-spacing density by a factor of ~30. This ought to improve the analysis' selectivity for specific life-cycle periods during the development and decay of individual convective cells.

In practice, the proportion of +CGs is extremely low in Florida storms (see Table 2) compared to certain other geographical regions. This study's LASA dataset has a +CG::-CG ratio of 0.014. This is not inconsistent with a recent comprehensive study [Carey, L. D. et al., 2003] of the relationship of severe storm reports to the CG polarity, which indicates that the association of predominantly positive-polarity storms to severe weather is evident in the Great Plains and upper Midwest, while Florida does not display this association. Therefore we caution that our present study, centered on Florida, cannot address the relationship of NBEs to +CGs, because the latter are not sufficiently represented in our Florida dataset.

To demonstrate the spatial relationship between NBE and CG events, we first examine the minimum distance of an event of one kind to an event of another. To do this, we use a sliding 11-pixel X 11-pixel window centered on the pixel containing any particular lightning event. We tally the minimum distance from the sliding window's central pixel to the closest pixel that contains a neighbor event of a given lightning type. This results in uneven sampling of isotropic distance, so we correct for that by normalizing with the number of possible samples in each isotropic-distance bin. Figure 3 shows the bias-corrected distribution of minimum distance to simultaneous neighbors, using 10-km isotropic-distance bins. Figure 3(a) shows the minimum distance of one polarity of NBE to the other polarity. The solid curve is the distribution of minimum distance from +NBEs (centered in the moving 11-pixel X 11-pixel window) to neighboring –NBEs. The dased curve is the distribution of minimum distance from -NBEs (centered in the moving 11-pixel X 11-pixel window) to neighboring +NBEs. It apparently is rare to have any

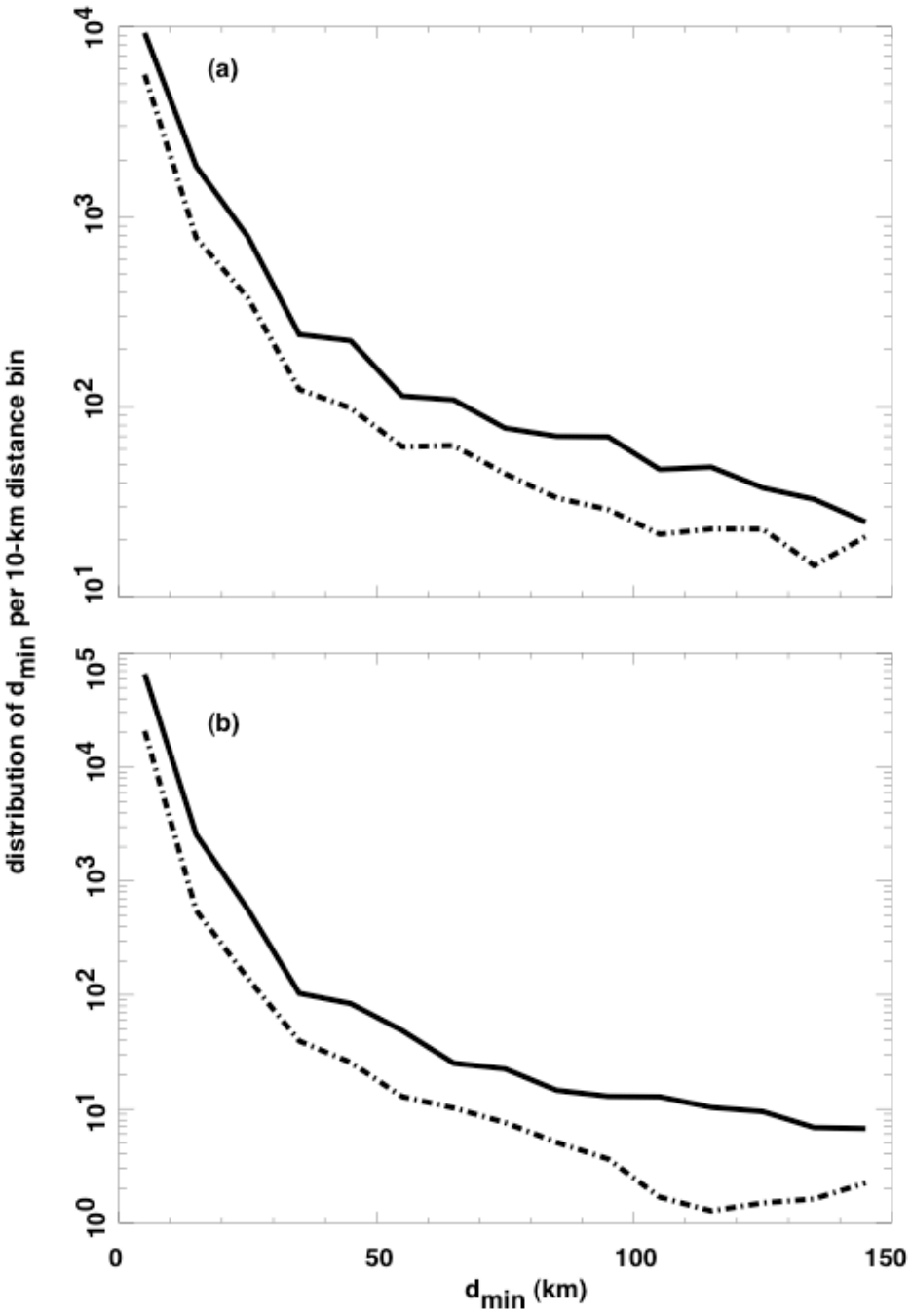

Figure 3: Distribution of minimum distance from key lightning events to neighboring lightning events, versus isotropic distance. (a) Solid curve: Key events = +NBEs, neighboring events = -NBEs. Dashed curve: Key events = -NBEs, neighboring events = +NBEs. (b) Solid curve: Key events = +NBEs, neighboring events = non-NBEs. Dashed curve: Key events = -NBEs, neighboring events = non-NBEs. The distributions have been corrected for the uneven sampling of isotropic distance (see text).

spatially association between simultaneous NBEs of opposite polarity. That is, each storm containing NBEs tends to contain only NBEs consistently of one polarity or another, but not both. The total number of +NBEs in this study is 79,068 (see Table 2), but the percentage of these +NBEs associated with simultaneous –NBEs within 150 km distance is only less than 15% (see Figure 3a, solid curve). A similar conclusion holds for –NBEs (see Figure 3a, dashed curve). Despite the tendency of NBE-producing storms to produce only one polarity of NBEs, the few cases (<15 %) of storms that produce both polarities tend to place them in close proximity (same pixel; see Figure 3a).

Figure 3(b) shows the minimum distance from +NBEs (solid curve) and from –NBEs (dashed curve) to non-NBEs (+CG & -CG & undetermined events). Each polarity of NBE is overwhelmingly likely to occur in a pixel that simultaneously contains at least one non-NBE lightning event. Thus, almost whenever NBEs occur, they do so in pixels containing "ordinary lightning". Thus NBEs are not an isolated phenomenon set apart from ordinary lightning, but occur almost without exception in places where ordinary lightning simultaneously (within 10 minutes) occurs.

The next step in testing the spatial relationship between NBEs and ordinary lightning is to estimate the covariances versus spatial and temporal separation. We use the same 11-pixel X 11-pixel sliding window centered on the pixel containing the key event. We look for neighbors of the key event in all 121 pixels in the 11-pixel X 11-pixel sliding window. However, rather than note the minimum distance to a neighbor, we take the product of the central-pixel population of key events times the populations of all 121

pixels in the sliding window. This gives 121 products, representing discrete sampling of different separations. We then sum that product matrix over all 300-sec time steps and over all days in the four-year period 1999-2002. Finally, we re-order the 121-element matrix elements by isotropic distance from the key event.

Based on the summed population-product matrix, we calculate the normalized correlation versus isotropic separation. Because Florida (see Figure 2) is not isotropic but rather is a peninsula, and tends to impose some degree of N-S elongation on the storm activity, the spatial correlation shows slight departures from isotropy.

Figure 4 shows three correlation functions, truncated to highlight the correlation range 0.0 to 0.4. The heavy solid curve is the autocorrelation of –CG populations, normalized to unity at zero separation. The light solid curve is the autocorrelation of +NBE populations, also normalized to unity at zero separation. The heavy dashed curve is the cross-correlation of –CG populations with +NBE populations. The cross-correlation's zero-separation value is only 29% (see Table 4), but the heavy dashed curve has been artificially amplified by 1/0.29 to allow ready comparison with the two autocorrelation functions.

The fine-scale irregularities in all three curves in Figure 4 are due to the slight anisotropies in the correlation matrix. Despite this anisotropy, all three correlations fall off clearly with increasing isotropic separation. The –CG autocorrelation (heavy solid curve) is wider than the +NBE autocorrelation (light solid curve), below the 0.2

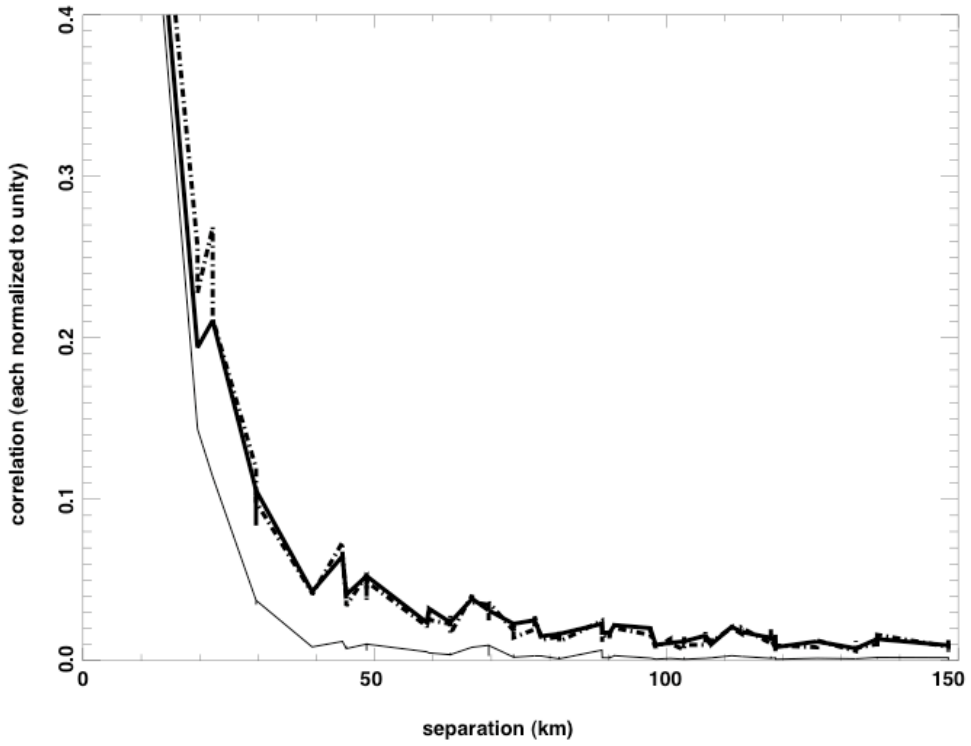

Figure 4: Equal-time, spatial correlation functions versus isotropic separation. All curves are truncated at 0.4 even though their highest point (at zero separation) is unity. Heavy solid curve: Autocorrelation function of –CG pixel occupancy. Light solid curve: Autocorrelation function of +NBE pixel occupancy. Heavy dashed curve: Cross-correlation function of –CG with +NBE pixel occupancies, multiplied by factor 1/0.29 to compensate for 29% correlation at zero separation. The fine-scale irregularities are caused by anisotropies (see text).

correlation level. The cross correlation mimics the wider autocorrelation. These relationships indicate that NBEs tend to occur in spatially tighter sub-zones of the storms compared to ordinary lightning. The 29% cross-correlation of +NBEs with –CGs in Florida is highly significant, as the statistical noise (tail value at right end of heavy dashed curve) is only < 0.02. The significant, but partial, cross-correlation is consistent with earlier findings of a statistical, though not case-by-case, proportionality between CG flash rates and NBE event rates [Suszcynsky, D. M. and Heavner, M. J., 2003]. The behavior of the –NBE pixel populations (not shown) is similar to that of the +NBEs, although the –NBEs' peak correlation with –CGs is only 16% (see Table 4). The –NBE autocorrelation is almost identical in shape and width with the +NBE autocorrelation (Figure 3, light solid curve). All the zero-separation correlation coefficients are listed in Table 4.

The results in Figures 3 and 4 have shown the equal-time correlations as a function of spatial separation. Now we reverse the procedure and examine the zero-separation correlations as a function of temporal separation. Figure 5 shows the temporal autocorrelations for (a) –CGs, (b) +NBEs, and (c) –NBEs. In each panel, the solid curve is without any spatial smoothing, while the dashed curve is with 5-pixel X 5-pixel (approximately 100-km) spatial smoothing. The halfwidth to 1/e for –CGs is about 2500 s without spatial 100-km smoothing, and about twice that with spatial 100-km smoothing. The halfwidth to 1/e for each type of NBE is about 1200 s without spatial 100-km smoothing, and only about 25% more with spatial 100-km smoothing. Two features are apparent: First, the duration of NBE occurrences during a given storm tends to be only

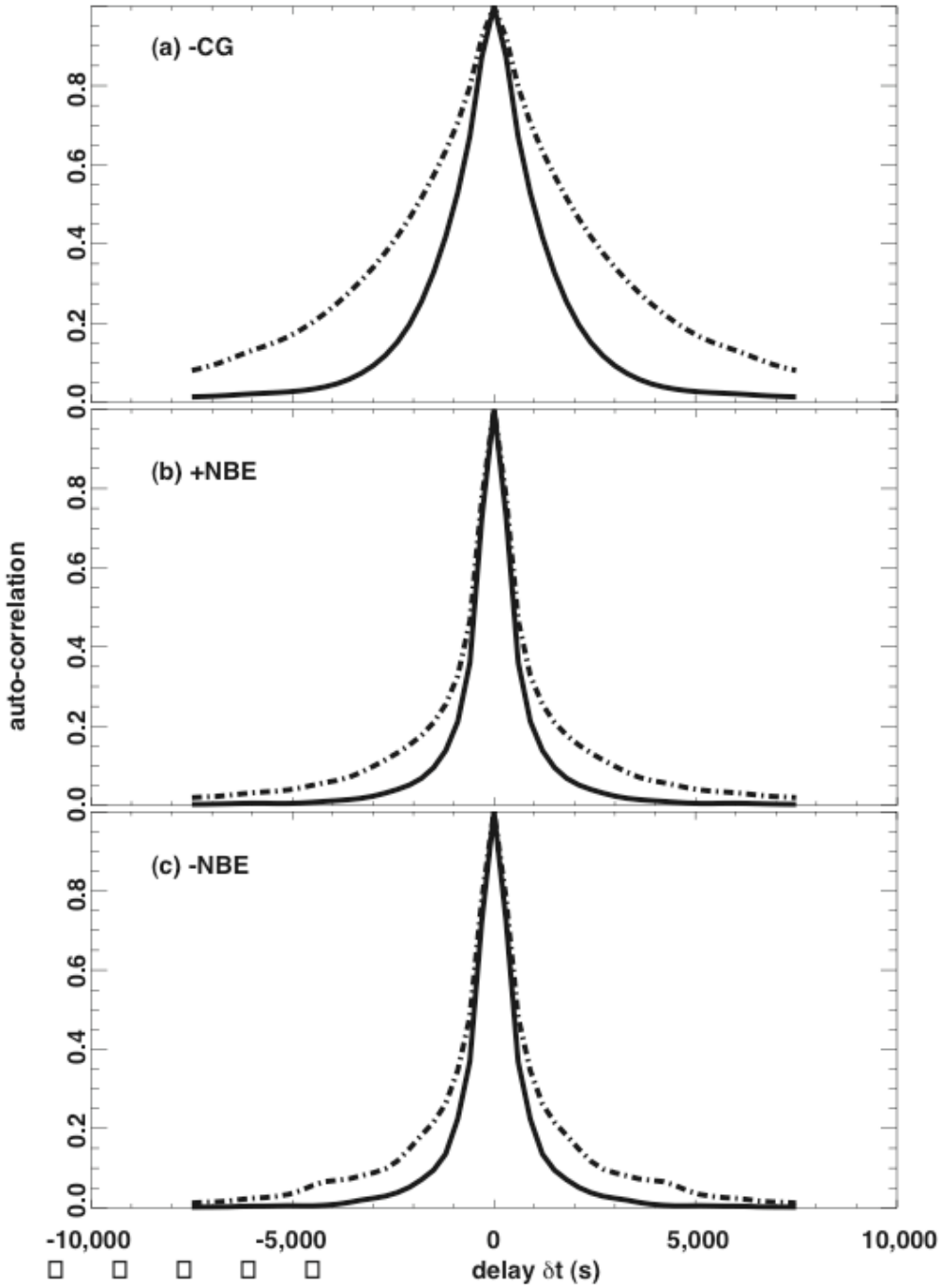

Figure 5: Zero-separation, temporal autocorrelation functions for (a) –CG pixel occupancies, (b) +NBE pixel occupancies, and (c) –NBE pixel occupancies. Solid curves: Without further spatial averaging. Dashed curves: With prior spatial smoothing by 5-pixels X 5-pixels (~100-km X 100-km).

half the duration of –CG occurrences in the same storm. Second, the distribution of –CGs is two-fold wider in time if we first average over 100 km spatially, whereas the distribution of NBEs undergoes 25% further widening in time. This indicates that –CGs appear in more phases of a developing/advecting storm complex than do NBEs (of either polarity.)

Lagged (as a function of lag Δt) correlations can also address whether one type of lightning event tends to precede, or follow, another type during the development of storms. Figure 6 shows (heavy dashed curve) the correlation of (a) -CG(t) with +NBE(t+Δt), (b) -CG(t) with -NBE(t+Δt), and (c) +NBE(t) with -NBE(t+Δt). In each panel the heavy solid curve is the first type's auto-correlation, the light solid curve is the second type's auto-correlation, and the heavy dashed curve is the cross-correlation. The latter is artificially multiplied by the inverse of the cross-correlation coefficient (see Table 4) to allow ready comparison to the auto-correlation functions. The autocorrelations in Figure 6 are the same as the auto-correlations in Figure 5 and are repeated to provide a comparison to the cross-correlations.

Figure 6 indicates that there is no systematic lag of NBEs (of either polarity) with respect to –CGs. Although NBEs (of either polarity) occur during a smaller duration of the storm lifecycle than do –CGs, the NBE occurrences are not systematically advanced or retarded with respect to the temporal centroid of –CGs. Similarly, to the small extent that –NBEs coexist with +NBEs (correlation: 11%), they have no systematic lag relationship (Figure 6c).

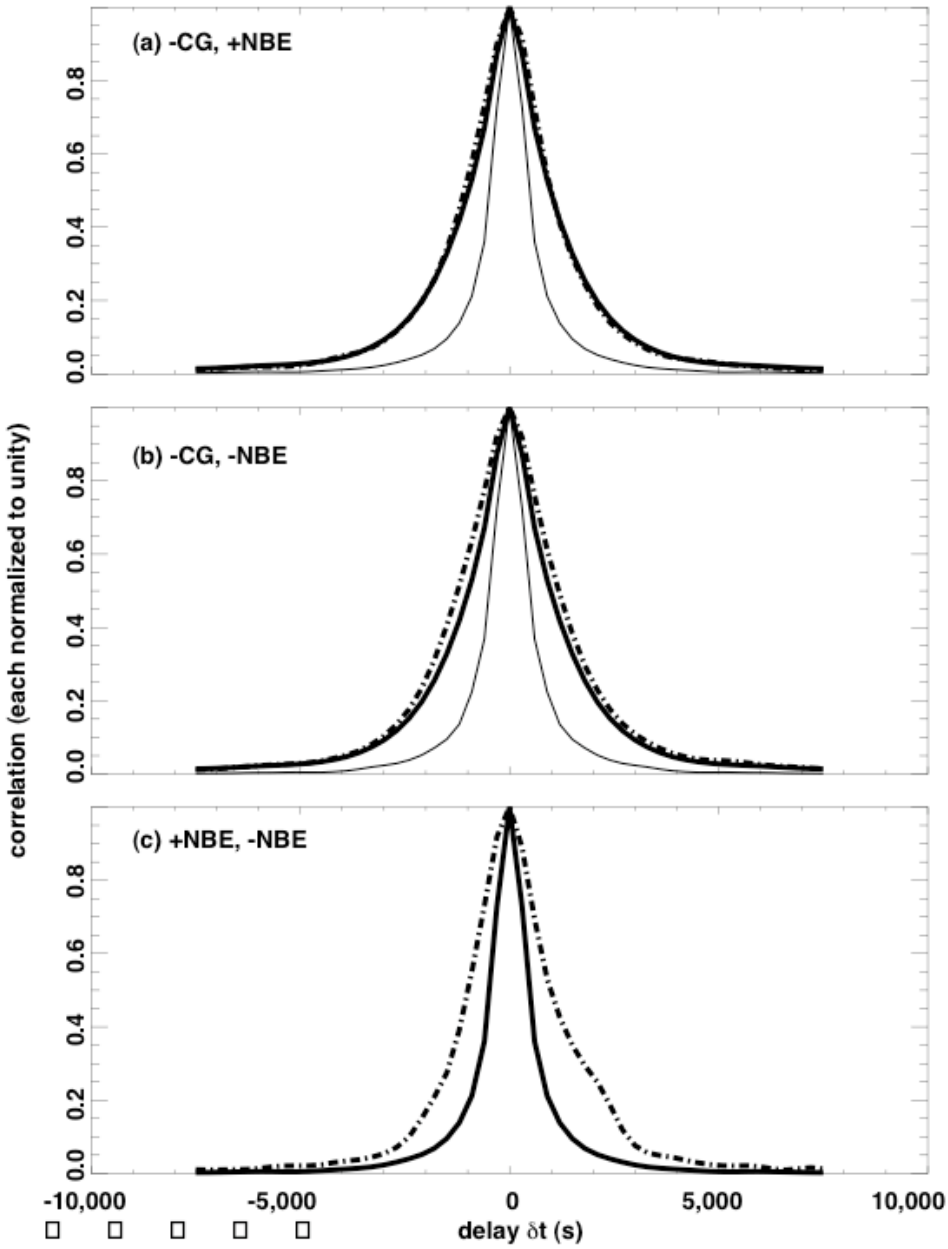

Figure 6: In each panel, two autocorrelation functions repeated from Figure 5 (heavy and light solid curves) and one cross-correlation function (heavy dashed curve), for (a) –CGs and lagged +NBEs (multiplied by factor 1/0.29), (b) –CGs with lagged –NBEs (multiplied by factor of 1/0.16), and (c) +NBEs with lagged –NBEs (multiplied by factor of 1/0.11).

4. Comparison of lightning incidence to cloud-top temperature data

The purpose of this section is to determine whether NBEs behave as do –CGs with respect to their spatial relationship to clouds. Ordinary lightning is far more likely to be accompanied by high (i.e., cold) cloud tops [Williams, E. R., 2001] than to be accompanied by low (i.e. relatively warm) cloud tops. Do NBEs behave similarly? We answer this with infrared cloud maps. These cloud maps at 10.7 microns (GOES East, IR channel #4) reveal the cloud-top temperature. The cloud-top temperature then serves as a crude cloud-top altimeter, assuming that the inferred temperature is in equilibrium with the environmental thermocline. This altimetry can be performed only in the monotonic portion of the thermocline, from ground to the tropopause. It is not expected that thunderclouds will occur in equilibrium above the tropopause, although a few km of overshoot can occur transiently for exceptionally vigorous convection [Williams, E. R., 2001]. At any rate, for cloud parcels that are in vertical motion and hence not in equilibrium with their surroundings, the altitude estimate from cloud-top temperature is erroneous.

The thermocline varies both diurnally and seasonally. Figure 7 shows temperature versus height from all radiosondes launched out of Cape Kennedy, Florida during 2001, regardless of local time and season. The radiosonde observations are provided by the Forecast Systems Laboratory of NOAA (http://raob.fsl.noaa.gov). Each of the 44,733 dots in Figure 7 is a reported temperature. The dots follow a well-defined and reproducible thermocline. Some anomalous outliers are obvious; all 2001 data are included without editing, including points with obvious errors. Superimposed on the data

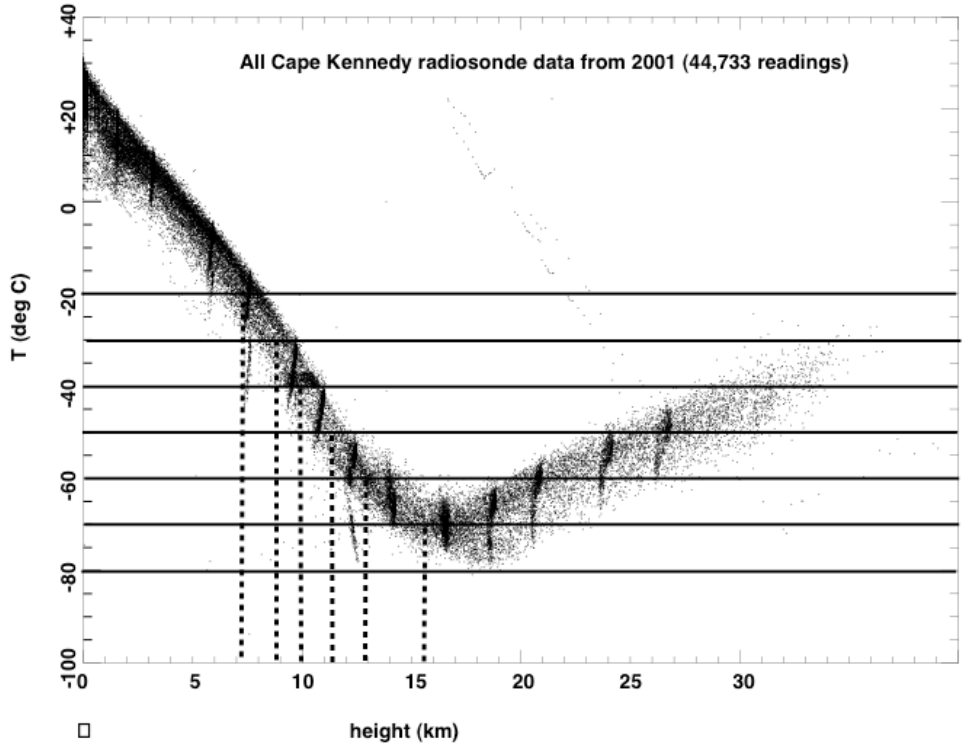

Figure 7: Cape Kennedy radiosonde temperature measurements versus height for all soundings during 2001. Spurious artifacts are included. Data from NOAA/Forecast Systems Laboratory (see text).

are isotherms (horizontal lines) from –20 deg C to –80 deg C, in steps of 10 deg C. Each isotherm's intersection with the observed thermocline is marked by a dashed vertical line at constant altitude. It is seen that the temperature tropopause occurs around ~15-km altitude and at a temperature around –70 deg C. Thus it would not be expected to see thunderclouds above 15 km in equilibrium with their environment.

The first question is, do the NBEs occur at heights that are consistent with their being in the troposphere? If not, it would be difficult to associate them with thunderstorm phenomena. The NBE waveform often permits the automated retrieval of emission height [Smith, D. A. et al., 2004]. This was possible in about 2/3 of the NBEs used in this analysis with IR-imagery support (see Table 3). Figure 8 shows the distribution of inferred NBE emission height based on automated processing of the waveform. The distribution peaks at 13-14 km altitude. Over 80% of the NBEs are emitted below 15 km. However, the <20% of NBEs in this distribution that are emitted in the range 15-20 km altitude are unlikely to be completely explainable as measurement artifacts. We believe our altitude-measurement uncertainties are <2 km, so it is likely that at least some of these events are truly occurring above the nominal tropopause. It remains unclear whether these high-altitude NBEs occur in clear air above the cloud tops (as in "blue jets" [Wescott, E. M. et al., 1998]) or occur in overshooting clouds that transiently exceed the equilibrium tropopause height [Williams, E. R., 2001].

Having determined that the NBEs tend to occur in the upper troposphere, we now examine what their relationship is with cloud heights as inferred from the cloud-top

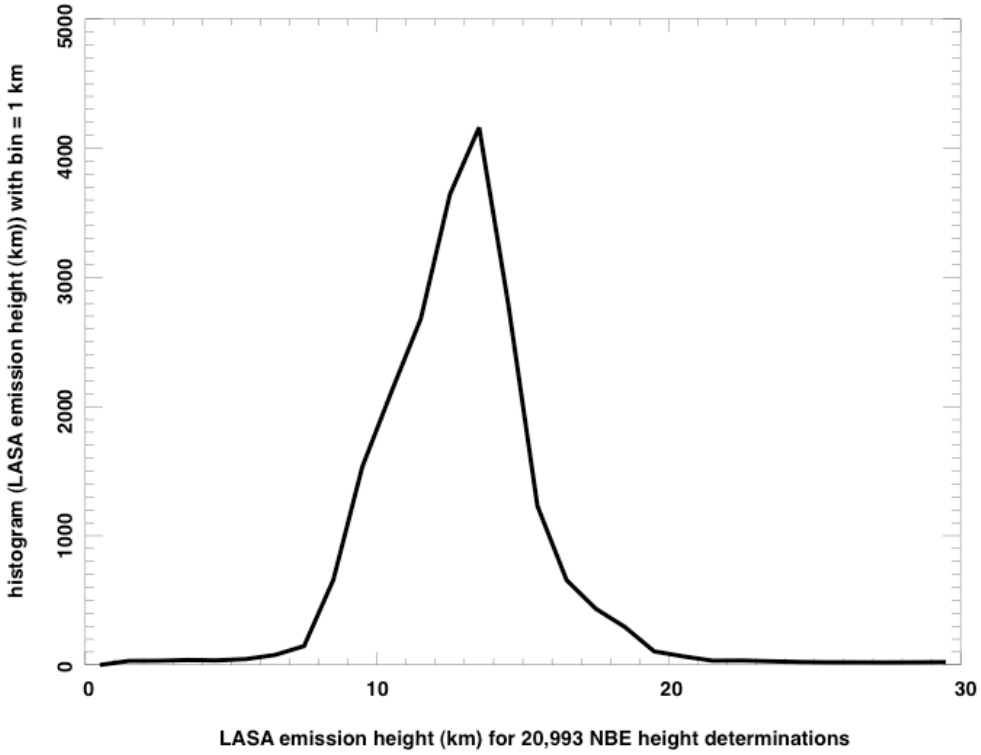

Figure 8: Distribution of NBE emission height for 20,993 NBE waveforms that allowed automated retrieval of ionospheric and emission heights (see text).

temperature. For this purpose, we do not use the lightning-event pixellation, but instead use the exact observed location of each lightning event. We use the pixels of the GOES-East image (which do *not* coincide with our 0.2-deg X 0.2-deg lightning pixellation) and compute the inferred cloud-top temperature for those pixels. For each lightning event detected by LASA, we gather all the image pixels whose centers lie within both 30-km, and 100-km, -radius circles centered on the lightning location. We then build two statistics from the cloud-top temperatures within each of these circles: First, we tally the full distribution of cloud-top temperatures within the circle. Second, we tally the coldest cloud-top temperature within the circle. These two statistics are then accumulated over the entirety of LASA-located lightning events (see Table 3) for which there is GOES-East imagery.

Figure 9 shows histograms of the distribution of cloud-top temperatures proximal to lightning, summed over all the IR images in the archive. The light solid curve is for the background distribution over all pixels in the entire scene, regardless of proximity to lightning locations. The heavy solid curve is for those pixels with a 30-km-radius circle proximal to each lightning event. The heavy dashed curve is for those pixels within a 100-km-radius circle proximal to each lightning event. The lightning events in Figure 9(a) are non-NBEs (+CG & -CG & undetermined), while those in Figure 9(b) are the NBEs (of both polarities summed together).

First consider the background temperature distribution (light solid line) in both panels of Figure 9. Obviously it is the same curve in both Figures 9(a) and 9(b), because it is not

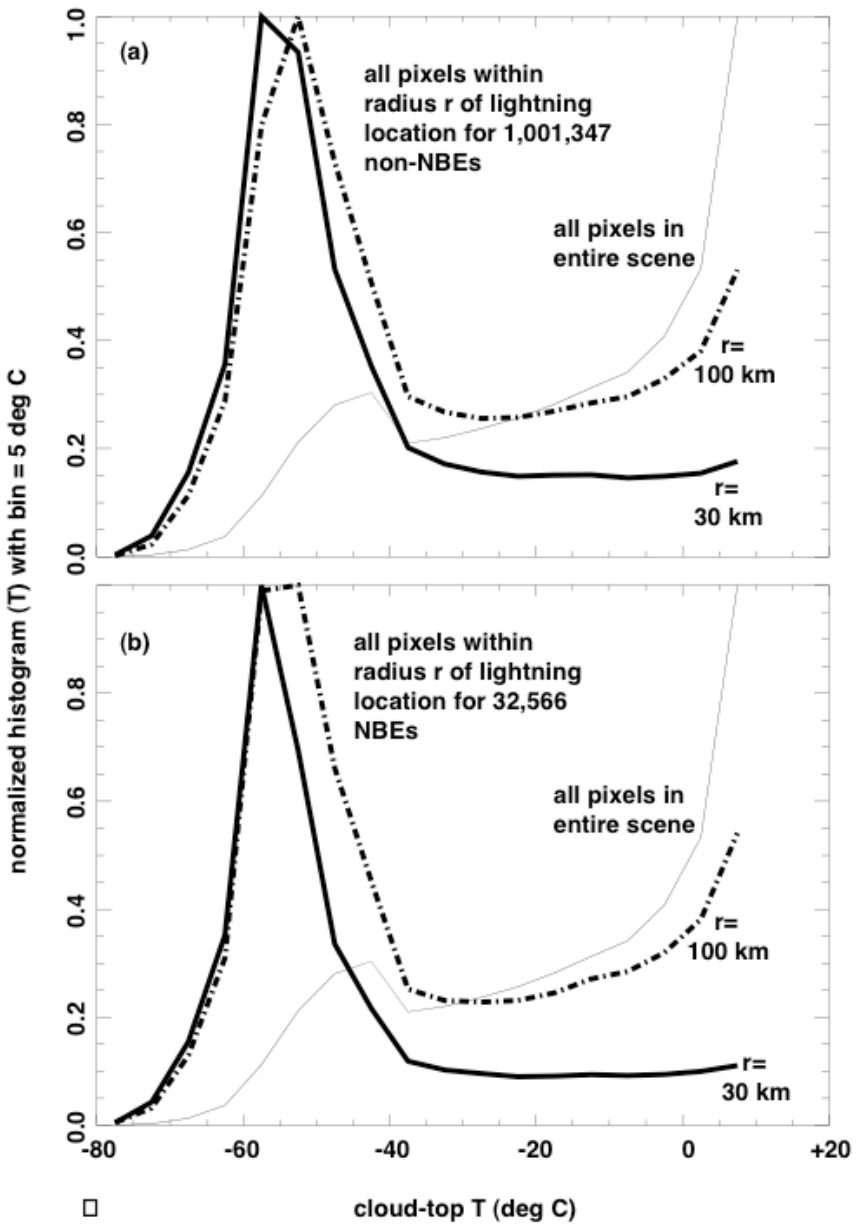

Figure 9: Distribution of cloud-top temperatures inferred from GOES-East IR (10.7-□m) imagery during times in 1999-2002 in which there was LASA data. Light solid curve: Background cloud distribution over entire Florida-area sub-image (see Figure 2). Heavy solid curve: Cloud distribution within 30-km proximity to each lightning event. Heavy dashed curve: Cloud distribution within 100-km proximity to each lightning event. (a) For non-NBE lightning. (b) For NBE lightning (both polarities).

conditioned by proximity to lightning. The steeply rising feature at the far right (high temperature) is the transition to clear skies. The smaller hump at –40 deg C to –50 deg C is the cloud signature. This cloud signature has a tail going out to –70 deg C, roughly as we would expect (see the radiosonde data in Figure 7) for deep convection.

Next, consider the distribution of cloud-top temperatures in proximity to either non-NBEs (Figure 9a) or NBEs (Figure 9b). The peak for either 30-km or 100-km proximity is located on the cold (left) tail of the background distribution, near –50 deg C to –60 deg C. According to the radiosonde thermocline (Figure 7), that corresponds to altitudes around 12 km. That is within the peak of the NBE altitude distribution inferred from the waveform data (Figure 8), so the two independent ways of constraining cloud height seem not to be radically inconsistent. For both non-NBEs (Figure 9a) and NBEs (Figure 9b), the distributions for r=30 km are colder than those for r=100 km. This is reasonable, in that the further away from the lightning location one allows the cloud pixel to be accumulated in the statistic, the more chance of including shallower (lower) clouds that are near, but not immediately associated with, the lightning. This also explains the higher "bridge" value for r=100 km in the transition region (-40 deg C to 0 deg C). Further from the lightning, there is more low cloud, broken cloud, or even clear sky.

Given that lightning can occur in compact updraft cells whose transverse size (<10 km) is not well resolved in GOES imagery, the use of 30-km-radius, and even moreso of 100-km-radius, circles around a given lightning event inevitably tends to include portions of the image that are not directly pertinent to the electrification/lightning process. In Figure

10, we show the distributions of the *single coldest* cloud pixel within these two radii. These single-coldest-pixel distributions are much narrower than the distributions of Figure 9 and entirely lack the "bridge" feature at T > -40 deg C. The centroid of the peak for either non-NBEs (Figure 10a) or NBEs (Figure 10b) is around –60 deg C. This corresponds to the 13-km height on the radiosonde data (Figure 7). Notice also that the single-coldest-pixel distribution remains significant right out to –70 deg C, corresponding to the nominal tropopause.

The cloud-top-temperature distributions in both Figures 9 and 10 indicate that, as regards affinity for cold cloud tops, NBEs behave roughly as do ordinary lightning events. Both non-NBEs and NBEs are highly selective for being near the coldest cloud tops possible, up to the limit imposed by the tropopause temperature. Both non-NBEs and NBEs are highly unlikely to occur within cloud environments warmer than –40 deg C. This is consistent with the consensus of observations reviewed elsewhere [Williams, E. R., 2001].

5. Summary and conclusions

We have examined the relationship of NBE lightning to ordinary (non-NBE) lightning, using the same detection system (LASA) for an unbiased comparison, over four years of observations within a tight geographical study area centered on Florida. This dataset comprises about three-million lightning events. We have compared the LASA data with cloud-top-temperature inferences from GOES-East IR images that are recorded within 15

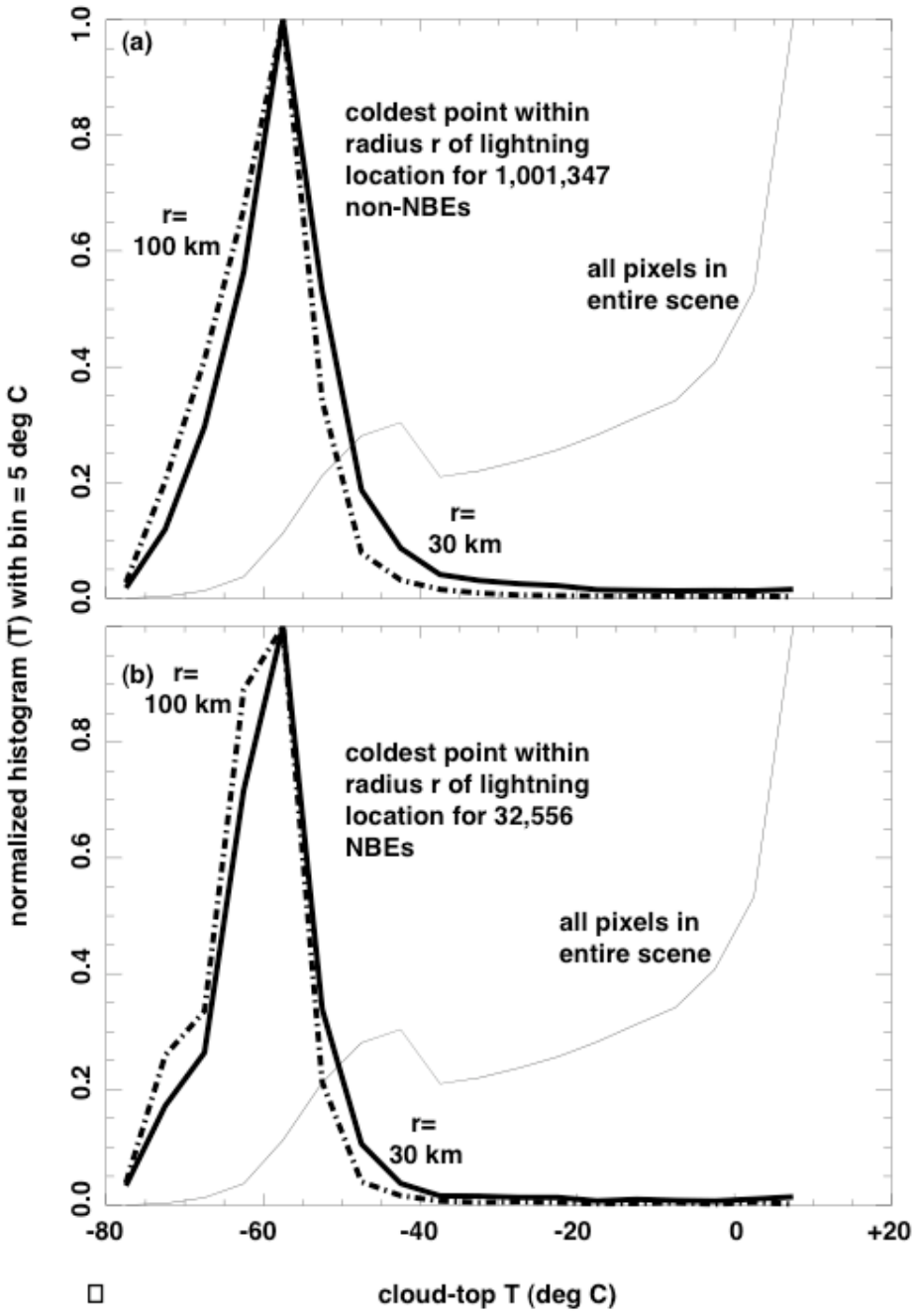

Figure 10: Light solid curve is identical to that in Figure 9, but heavy curves are distributions of *minimum* cloud-top temperature proximal to lightning events, within r=30 km (heavy solid curve) and within r=100 km (heavy dashed curve). (a) Lightning = non-NBEs; (b) lightning = NBEs.

minutes of any given lightning event. The IR-supported lightning events number over one-million. Our observations lead to the following conclusions:

(a) When a given thunderstorm gives rise to NBE discharges, the polarity of the discharge tends to be consistent for that storm. That is, a given storm is usually associated purely with +NBEs or purely with –NBEs, but not both (see Figure 3a).

(b) When a given thunderstorm gives rise to NBE discharges (regardless of polarity), that storm also gives rise to ordinary (non-NBE) lightning discharges (see Figure 3b).

(c) Spatially, NBEs occupy a more compact portion of a thunderstorm than do non-NBEs (see Figure 4). +NBEs and –NBEs are similarly compact in their appearance, though not in the same storms.

(d) During the development and migration of a thunderstorm, the non-NBEs are present for about twice as long as are the NBEs (see Figure 5). This does not depend on NBE polarity.

(e) Within thunderstorms, NBEs neither consistently precede nor consistently follow the centroid of non-NBE occurrences (see Figure 6).

(f) Most NBEs occur at altitudes within the upper troposphere. Fewer than 20% occur above the nominal tropopause, and virtually none above 20 km.

(g) The distribution of cloud-top temperatures proximal to the locations of both NBEs and non-NBEs is peaked at –50 deg C to –60 deg C (see Figure 9), corresponding to cloud-top heights in the upper troposphere. The cloud-top-temperature distribution for NBEs is essentially similar to the distribution for non-NBEs.

(h) The distribution of single-coldest-pixel cloud-top temperatures proximal to the locations of both NBEs and non-NBEs is peaked at –60 deg C (see Figure 10). The single-coldest-pixel cloud-top-temperature distribution proximal to NBEs is essentially similar to the distribution proximal to non-NBEs. Both NBEs and non-NBEs are almost never seen in cloud systems for which all cloud-top temperatures are warmer than –40 deg C within 30 km proximal to the lightning event.

In summary, the behavior of NBEs appears to be essentially the same as the behavior of non-NBEs, as regards selectivity for deep convective-cloud structures. As regards the timing and spatial relation of NBEs to non-NBEs in storms that contain both, NBE occurrence tends to cover less of the spatial extent or temporal lifetime of the storm. NBE occurrence does not appear to be a consistent precursor of non-NBE occurrence, and vice-versa. Therefore, in view of what we have found, it seems reasonable to assume that the extensive literature on the meteorological setting of "ordinary" lightning might also apply to NBE lightning. In particular, it appears reasonable to assume that NBEs as a remote-sensing proxy of severe convection might have a utility comparable to that of ordinary lightning, albeit in the context of radio VHF, not optical, detection techniques.

A limitation of this study is that Florida has too few +CGs to allow a determination of the relationship of NBEs and +CGs. Future work other than in Florida, e.g. in the Great Plains, will be required to address this question.

Acknowledgements

This work was conducted under the auspices of the United States Department of Energy, with support from the LANL/LDRD program. The LASA facility is the product of many years of effort by many staff, postdocs, and students at Los Alamos, without whose contributions the present work would not have been possible.

References

Boccippio, D. J., 2002: Lightning scaling relations revisited. *J. Atmos. Sci.*, **59,** 1086-1104.

Boccippio, D. J., W. J. Koshak, H. J. Christian, and S. J. Goodman, 1999: Land-ocean differences in LIS and OTD tropical lightning observations. *11th International Conference on Atmospheric Electricity*, Huntsville, Alabama, National Aeronautics and Space Administration (U. S.), 734-737.

Boccippio, D. J., K. Driscoll, W. Koshak, R. Blakeslee, W. Boeck, D. Buechler, H. Christian, and S. Goodman, 2000: The Optical Transient Detector (OTD): Instrument characteristics and cross-sensor validation. *J. Atmos. Oceanic Tech.*, **17,** 441-458.

Carey, L. D., S. A. Rutledge, and W. A. Petersen, 2003: The relationship between severe storm reports and cloud-to-ground lightning polarity in the contiguous United States from 1989 to 1998. *Mon. Wea. Rev.*, **131,** 1211-1228.

Christian, H. J., R. J. Blakeslee, D. J. Boccippio, W. L. Boeck, D. E. Buechler, K. T. Driscoll, S. J. Goodman, J. M. Hall, W. J. Koshak, D. M. Mach, and M. F. Stewart, 1999: Global frequency and distribution of lightning as observed by the Optical Transient Detector (OTD). *11th International Conference on Atmospheric Electricity*, Huntsville, Alabama, National Aeronautics and Space Administration (U. S.), 726-729.

Christian, H. J., R. J. Blakeslee, S. J. Goodman, D. A. Mach, M. F. Stewart, D. E. Buechler, W. J. Koshak, J. M. Hall, W. L. Boeck, K. T. Driscoll, and D. J. Boccippio, 1999: The Lightning Imaging Sensor. *11th International Conference on Atmospheric Electricity*, Global Hydrology and Climate Center, NASA Marshall Space Flight Center, Huntsville, Alabama, NASA.

Gurevich, A. V., K. P. Zybin, and R. A. Roussel-Dupré, 1999: Lightning initiation by simultaneous effect of runaway breakdown and cosmic ray showers. *Phys. Lett.*, **A254,** 79-87.

Jacobson, A. R., 2003: Relationship of intracloud-lightning radiofrequency power to lightning-storm height, as observed by the FORTE satellite. *J. Geophys. Res.*, **108,** 4204, doi:1029/2002JD002956.

——, 2003: How do the strongest radio pulses from thunderstorms relate to lightning flashes? *J. Geophys. Res.*, **108,** 4778, doi:10.1029/2003JD003936.

Jacobson, A. R. and X.-M. Shao, 2002: FORTE satellite observations of very narrow radiofrequency pulses associated with the initiation of negative cloud-to-ground lightning strokes. *J. Geophys. Res.*, **107,** 4661, doi:10.1029/2001JD001542.

Jacobson, A. R. and T. E. L. Light, 2003: Bimodal radiofrequency pulse distribution of intracloud-lightning signals recorded by the FORTE satellite. *J. Geophys. Res.*, **108,** 4266, doi:10.1029/2002JD002613.

Jacobson, A. R., S. O. Knox, R. Franz, and D. C. Enemark, 1999: FORTE observations of lightning radio-frequency signatures: Capabilities and basic results. *Radio Sci.*, **34,** 337-354.

Jacobson, A. R., K. L. Cummins, M. Carter, P. Klingner, D. Roussel-Dupré, and S. O. Knox, 2000: FORTE radio-frequency observations of lightning strokes detected by the National Lightning Detection Network. *J. Geophys. Res.*, **105,** 15,653.

Kirkland, M. W., D. M. Suszcynsky, J. L. L. Guillen, and J. L. Green, 2001: Optical observations of terrestrial lightning by the FORTE satellite photodiode detector. *J. Geophys. Res.*, **106,** 33,499-33,509.

Le Vine, D. M., 1980: Sources of the strongest rf radiation from lightning. *J. Geophys. Res.*, **85,** 4091-4095.

Light, T. E. L. and A. R. Jacobson, 2003: Characteristics of impulsive VHF lightning observed by the FORTE satellite. *J. Geophys. Res.*, **in press**.

Massey, R. S. and D. N. Holden, 1995: Phenomenology of transionospheric pulse pairs. *Radio Sci.*, **30,** 1645-1659.

Massey, R. S., D. N. Holden, and X.-M. Shao, 1998: Phenomenology of trans-ionospheric pulse pairs: Further observations. *Radio Sci*, **33,** 1755-1761.

Massey, R. S., S. O. Knox, R. C. Franz, D. N. Holden, and C. T. Rhodes, 1998: Measurements of transionospheric radio propagation parameters using the FORTE satellite. *Radio Sci.*, **33,** 1739-1753.

Nesbitt, S. W., E. J. Zipser, and D. J. Cecil, 2000: A census of precipitation features in the tropics using TRMM: Radar, ice scattering, and lightning observations. *J. Climate*, **13,** 4087-4106.

Petersen, W. A. and S. A. Rutledge, 1998: On the relationship between cloud-to-ground lightning and convective rainfall. *J. Geophys. Res.*, **103,** 14,025-14,040.

Roussel-Dupré, R. A., A. R. Jacobson, and L. A. Triplett, 2001: Analysis of FORTE data to extract ionospheric parameters. *Radio Sci.*, **36,** 1615-1630.

Shao, X.-M. and A. R. Jacobson, 2001: Polarization observations of broadband VHF signals by the FORTE satellite. *Radio Sci.*, **36,** 1573-1589.

——, 2002: Polarization observations of lightning-produced VHF emissions by the FORTE satellite. *J. Geophys. Res.*, **107,** 4430.

Smith, D. A., M. J. Heavner, A. R. Jacobson, X. M. Shao, R. S. Massey, R. J. Sheldon, and K. C. Wiens, 2004: A method for determining intracloud lightning and ionospheric heights from VLF/LF electric field records. *Radio Sci.*, **39,** doi:10.1029/2002RS002790.

Smith, D. A., K. B. Eack, J. Harlin, M. J. Heavner, A. R. Jacobson, R. S. Massey, X. M. Shao, and K. C. Wiens, 2002: The Los Alamos Sferic Array: A research tool for lightning investigations. *J. Geophys. Res.*, **107,** 10.1029/2001JD000502.

Smith, D. A., X. M. Shao, D. N. Holden, C. T. Rhodes, M. Brook, P. R. Krehbiel, M. Stanley, W. Rison, and R. J. Thomas, 1999: A distinct class of isolated intracloud lightning discharges and their associated radio emissions. *J. Geophys. Res.*, **104,** 4189-4212.

Suszcynsky, D., A. Jacobson, J. Fitzgerald, C. Rhodes, E. Tech, and D. Roussel-Dupre, 2000: Satellite-based global lightning and severe storm monitoring using VHF receivers. *EOS, Trans. Am. Geophys. Union*, **81,** F91.

Suszcynsky, D. M. and M. J. Heavner, 2003: Narrow Bipolar Events as indicators of thunderstorm convective strength. *Geophys. Res. Lett.*, **30,** 1879, doi:10.1029/2003GL017834.

Suszcynsky, D. M., T. E. Light, S. Davis, M. W. Kirkland, J. L. Green, and J. Guillen, 2001: Coordinated Observations of Optical Lightning from Space using the FORTE Photodiode Detector and CCD Imager. *J. Geophys. Res.*, **106,** 17,897-17,906.

Suszcynsky, D. M., M. W. Kirkland, A. R. Jacobson, R. C. Franz, S. O. Knox, J. L. L. Guillen, and J. L. Green, 2000: FORTE observations of simultaneous VHF and optical emissions from lightning: Basic Phenomenology. *J. Geophys. Res.*, **105,** 2191-2201.

Thomas, R. J., P. R. Krehbiel, W. Rison, T. Hamlin, J. Harlin, and D. Shown, 2001: Observations of VHF source powers radiated by lightning. *Geophys. Res. Lett.*, **28,** 143-146.

Toracinta, E. R. and E. Zipser, 2001: Lightning and SSM/I-ice-scattering mesoscale convective systems in the global tropics. *J. Appl. Meteor.*, **40,** 983-1002.

Toracinta, E. R., D. J. Cecil, E. J. Zipser, and S. W. Nesbitt, 2002: Radar, passive microwave, and lightning characteristics of precipitating systems in the tropics. *Mon. Wea. Rev.*, **130,** 802-824.

Ushio, T., S. J. Heckman, D. J. Boccippio, H. J. Christian, and Z.-I. Kawasaki, 2001: A survey of thunderstorm flash rates compared to cloud top height using TRMM satellite data. *J. Geophys. Res.*, **106,** 24,089-24,095.

Wescott, E. M., D. D. Sentman, M. J. Heavner, D. L. Hampton, and O. H. Vaughan, Jr., 1998: Preliminary results from the Sprites94 aircraft campaign: Blue Jets. *Geophys. Res. Lett.*, **22,** 1209-1212.

Willett, J. C., J. C. Bailey, and E. P. Krider, 1989: A class of unusual lightning electric field waveforms with very strong high-frequency radiation. *J. Geophys. Res.*, **94,** 16255-16267.

Williams, E., D. Rosenfeld, N. Madden, J. Gerlach, N. Gears, L. Atkinson, N. Dunneman, G. Frostrom, M. Antonio, B. Biazon, R. Camargo, H. Franca, A. Gomes, M. Lima, R. Machado, S. Manhaes, L. Nachtigall, H. Piva, W. Quintiliano, L. Machado, P. Artaxo, G. Roberts, N. Renno, R. Blakeslee, J. Bailey, D. Boccippio, A. Betts, D. Wolff, B. Roy, J. Halverson, T. Rickenbach, J. Fuentes, and E. Avelino, 2002: Contrasting convective regimes over the Amazon: Implications for cloud electrification. *J. Geophys. Res.*, **107,** 8082, doi:10.1029/2001JD000380.

Williams, E. R., 2001: Chapter 13: The Electrification of Severe Storms. *Severe Convective Storms*, C. A. I. Doswell, Ed., American Meteorological Society.

Zipser, E. J., 1994: Deep cumulonimbus cloud systems in the tropics with and without lightning. *Mon. Weather Rev.*, **122,** 1837-1851.

Zipser, E. J. and K. R. Lutz, 1994: The vertical profile of radar reflectivity of convective cells: A strong indicator of storm intensity and lightning probability? *Mon. Weath. Rev.*, **122,** 1751-1759.